Micro-Raman spectroscopy for the detection of stacking fault density in InAs and GaAs nanowires

Rawa Tanta,[1] Caroline Lindberg,[1] Sebastian Lehmann,[2] Jessica Bolinsson,[1,*] Miguel R. Carro-Temboury,[3] Kimberly A. Dick,[2,4] Tom Vosch,[3] Thomas Sand Jespersen,[1,†] and Jesper Nygård[1]

[1]*Center for Quantum Devices and Nano-Science Center, Niels Bohr Institute, University of Copenhagen, Universitetsparken 5, 2100 Copenhagen, Denmark*

[2]*Solid State Physics, Lund University, S-22100, Lund, Sweden*

[3]*Nano-Science Center, Department of Chemistry, University of Copenhagen, Universitetsparken 5, 2100 Copenhagen, Denmark*

[4]*Centre for Analysis and Synthesis, Lund University, Box 124, S-22100, Lund, Sweden*

(Received 16 August 2017; published 19 October 2017)

We investigate the relation between crystal stacking faults in individual wurtzite InAs and GaAs nanowires and the intensity of the forbidden longitudinal optical (LO) phonon mode in the Raman spectra. Micro-Raman spectroscopy and transmission electron microscopy are combined on the same individual nanowires to evaluate the LO mode intensity as a function of the stacking fault density. A clear increase in the LO mode intensity was observed when the stacking fault density was increased. Our results confirm the utility of Raman spectroscopy as a powerful tool for detecting crystal defects in nanowires.

DOI: 10.1103/PhysRevB.96.165433

I. INTRODUCTION

In the past decades the interest in semiconductor nanowires (NWs) has been steadily increasing. Within fundamental science, the inherent nanoscale confinement combined with the flexibility in material composition [1] and contact materials has led to a number of breakthroughs in quantum transport [2–6], with the demonstration of topologically nontrivial phases in strong spin-orbit nanowires [7,8] as an important recent example. Also, towards applications in technology the high surface-to-volume ratio enables efficient sensors [9] and promising performance of both photovoltaic devices [10] and field-effect transistors [11,12].

The important class of binary semiconductors such as GaAs, InAs, InSb, InN, and SiC can form in both the zinc-blende (ZB) and the wurtzite (WZ) crystal structure [13]. While the two phases differ only in the stacking sequence they have different symmetries and can have different optical [14], vibrational [15], mechanical [16], and electronic [17] properties. Nanowires grown by the conventional vapor-liquid-solid method [18] can be of high crystal quality, however, typical structures usually exhibit a varying number of randomly placed interruptions of the crystal stacking sequence, which can lead to an undesired decrease in device performance. As an important example, indium arsenide in the bulk form is found only in the ZB structure, while in the nanowire geometry the WZ structure is formed, with an increasing fraction for smaller nanowire diameters [19] as well as for tuned growth parameters [20,21]. Electrically, the ZB phase has a predicted band gap that is ∼100 meV lower than that of the WZ phase [17], and controlled WZ inclusions have been used to provide confinement for quantum dot structures [22,23]. Most often, however, stacking faults (SFs) are undesirable and will lead to random potential fluctuations and a degradation of device performance [24,25].

Stacking faults and polytypism in NWs are commonly investigated by high-resolution transmission electron microscopy (TEM). TEM is, however, incompatible with the common geometries of NW devices, and SF characterization techniques based on scanning electron microscopy (SEM) [23] or optical spectroscopy [26] have recently been investigated. Raman spectroscopy has emerged as a powerful noninvasive tool for probing the vibrational properties of nanostructures on substrates compatible with typical three-terminal electronic devices. Polarized Raman spectroscopy is commonly used to characterize crystal structure and SFs in NWs [27], and also temperature-dependent Raman measurements provide information on the relative WZ/ZB content [28]. Structural characterization has also been demonstrated by studying the so-called E_2 mode characteristic of the WZ structure [15,29].

Here we are investigating WZ InAs and GaAs nanowires, where the dominating stacking defects are small ZB segments. We present an extensive study of the consequence of SFs for the spatially resolved Raman spectrum, and by using substrates compatible with both TEM and Raman spectroscopy we correlate the results with high-resolution TEM images on the same individual NWs. We find the intensity of the longitudinal optical (LO) mode, which is forbidden by symmetry of the WZ crystal, to be related to the density of stacking faults. We investigate the polarization and excitation energy dependence of the SF response and we relate the observed LO mode to scattering from (111) planes of the ZB inclusions where the LO mode is allowed. This conclusion is consistent with a control experiment on ZB InAs NWs which were intentionally twinned and thus correspond to the limit where the entire NW consists of ZB inclusions. Possible contributions to the LO intensity due to electronic resonances were studied by repeating the measurements for GaAs NWs [15] which have the same crystal structure but different resonance conditions. The results were consistent with the InAs findings.

II. METHODOLOGY

Following the vapor-liquid-solid (VLS) approach, InAs NWs were grown by metal organic vapor phase epitaxy

*Present address: Tetra Pak Solutions AB, Ruben Rausings gata, SE-221 86 Lund, Sweden.

†tsand@fys.ku.dk

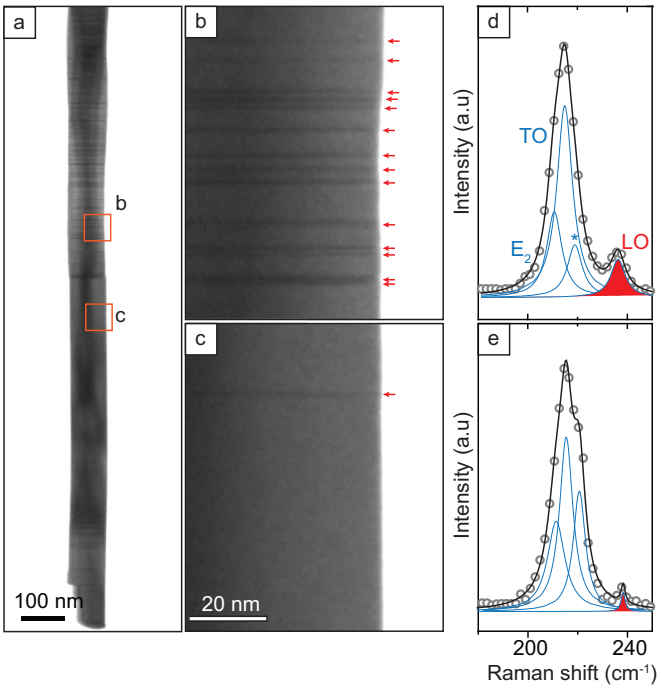

FIG. 1. (a) TEM bright-field overview image of an InAs nanowire with stacking variations. (b), (c) Higher-magnification images of areas marked in (a) with high and low densities of stacking faults (indicated by arrows), respectively. (d), (e) Raman spectra (circles) of the areas in (b) and (c) recorded with 514.5 nm excitation and polarization parallel to the NW axes for a power density of 390 kW/cm^2. Lorenzian fits of the spectra are shown and the LO mode is highlighted in red for clarity.

(MOVPE) in an AIXTRON 3 × 2″ close-coupled showerhead system operated at a pressure of 100 mbar and a total H_2 carrier gas flow of 8 standard liters per minute. Au aerosols with diameters of 80 nm were deposited onto $(\bar{1}\bar{1}\bar{1})$-oriented epi-ready InAs wafers at nominal densities of 1-2 μm^{-2} [30]. Before initiating NW growth an annealing step was carried out at a temperature of 550° C in an AsH_3/H_2 ambience with an AsH_3 molar fraction of $\chi_{AsH_3} = 2.5 \times 10^{-3}$. Nanowire growth was carried out at 470° C and a trimethylindium (TMIn) molar fraction of $\chi_{TMIn} = 1.8 \times 10^{-6}$. First, a stem was grown for 240 s with an AsH_3 molar fraction of $\chi_{AsH_3} = 1.1$–1.3×10^{-4}, and subsequently, AsH_3 was set for either wurtzite or zinc-blende growth conditions [20]. For growth of InAs NWs with a graded stacking defect density the growth was sequenced into five steps setting the AsH_3 molar fractions to $\chi_{AsH_3} = 2.3 \times 10^{-5}$, 4.5×10^{-5}, 6.8×10^{-5}, 1.4×10^{-4}, and 2.7×10^{-4} and the growth times to 900, 750, 600, 450, and 300 s, respectively. Finally, the reactor was cooled under hydrogen after turning off the TMIn supply. The resulting InAs NWs attain the WZ crystal structure, are ∼80 nm in diameter and ∼3 μm in length, and exhibit a variation in SF density along the NW. A typical NW is shown in the TEM image in Fig. 1(a). Zinc-blende InAs NWs with periodic twinning [22] were grown at a set temperature of 480° C for 30 min under an AsH_3 molar fraction of 5×10^{-4} and cooled down to 300° C in an AsH_3/hydrogen mixture with $\chi_{AsH_3} = 2.5 \times 10^{-3}$. A typical example is shown in Fig. 5(b).

In addition, GaAs NWs were grown in a Varian Gen II solid-source MBE system with Ag as seed particles [31]. Ag particles were generated by annealing an ∼1 nm Ag film on a GaAs $(\bar{1}\bar{1}\bar{1})$-oriented epi-ready wafer under an As_2 overpressure at 600° C for 10 min. Nanowires were grown at 600° C with an As/Ga flux ratio of 9 and a growth rate of 0.75 μm/h. Growth was performed for 1 h before cooling the substrate under As_2 overpressure. The NWs are ∼200 nm wide and ∼1.5 μm long. A typical example is shown in Fig. 6(a).

Structural characterization was carried out using a Philips CM20 TEM operated at 200 kV providing the overall crystal structure by selective area diffraction and the distribution of SFs was extracted by manual counting on images such as presented in Figs. 1(b) and 1(c). For detailed analysis of the NW structure high-resolution images were acquired with a JEOL 3000F microscope operated at 300 kV.

Raman measurements on individual NWs were performed using a micro-Raman setup in backscattering geometry. For excitation we used the 514.5 and 488 nm lines of an argon-ion laser (CVI Melles-Griot 35MAP431-200) and a HRR170-HeNe 632.8 nm laser. The beam was focused in an inverted confocal microscope by a 100×, 1.3-NA oil immersion objective onto a diffraction-limited spot. A $\lambda/2$ plate was installed before the microscope to control the polarization angle with respect to the NW axes. Lateral positioning and scanning with nanometer precision were enabled by a piezo-scanning stage (Physik Instrument P5173CL). Raman spectra were collected using a Princeton Instruments SPEC 10:100 B/LN-eXcelon CCD detector and an SP 2356 spectrometer with 1200 g/mm grating. The power of the excitation laser was carefully kept below the threshold of oxidation effects [32].

To enable a correlation of TEM and Raman measurements on the same individual NWs a 50 nm thick Si_3N_4 membrane was used as substrate [33]. Al (5 nm) or Al/Au (3/0.5 nm) was deposited on the back side of the membrane for GaAs and InAs NWs, respectively, to allow effective heat dissipation. In both cases of InAs and GaAs NWs, five and four wires, respectively, were fully mapped by TEM, allowing counting of SFs. Subsequently, Raman spectra were recorded for excitation polarization parallel and perpendicular to the NW axes, at different positions along the NW as marked on the optical images of the Raman microscope. Finally, the stacking defect density was quantified at the positions of the Raman spectra in 250 nm long segments. An SF was defined as any interruption of the atomic bilayer sequence regardless of the segment type or size. From HRTEM imaging with atomic-scale resolution of 96 SFs, it was found that 93% of the SFs have a size of 3 ± 1 atomic bilayers, mostly in the form of ZB inclusions.

III. RESULTS

A. InAs nanowires

According to the Raman selection rules for the WZ structure the zone-center LO phonon is forbidden in the backscattering geometry of the side facets of a NW grown along the [0001] crystal direction [34]. Imperfections and electronic resonances may, however, activate the LO mode, and in this study we use it as an indication of the SF density. To this end, InAs NWs were intentionally grown with an increasing SF density along the NW [see Fig. 1(a)]. The NWs were grown in the WZ

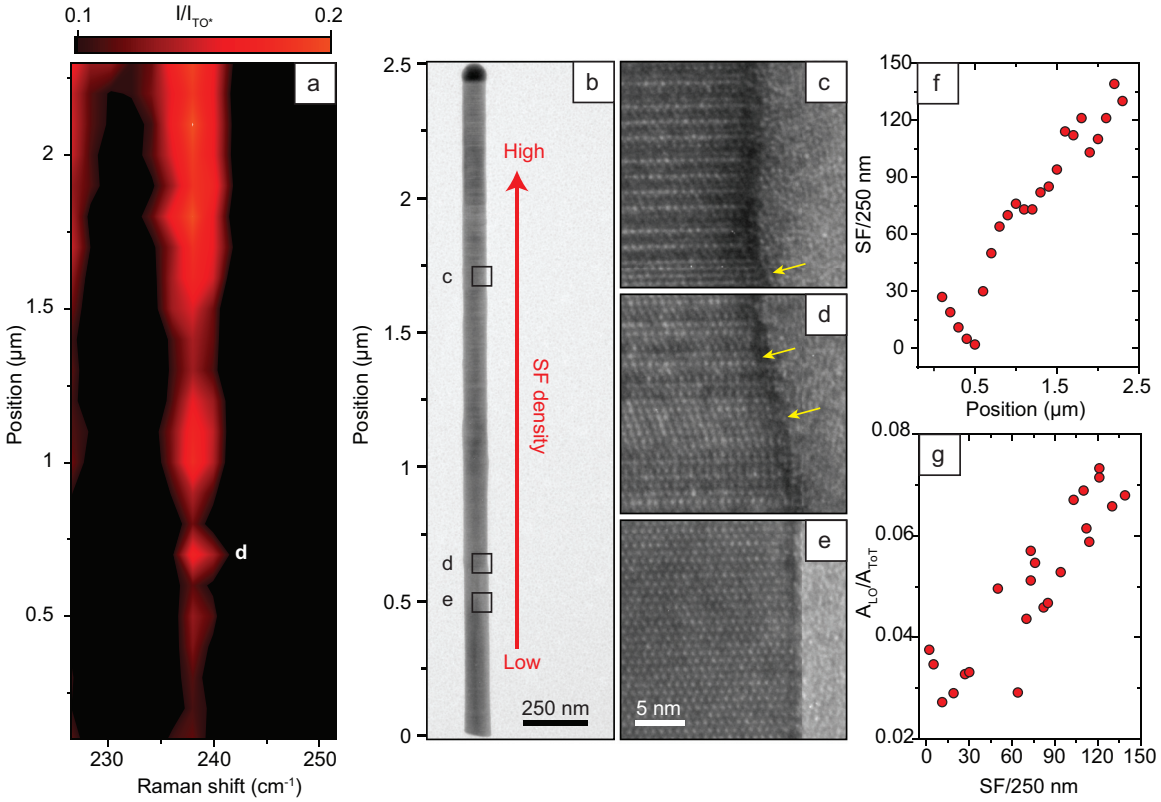

FIG. 2. (a) Perpendicularly polarized Raman scan of the InAs NW shown in (b) at 488 nm excitation, normalized to the TO* peak, which represents a combined peak of the E_2, $A_1 + E_1$(TO), and $*$ peaks. (b) TEM image of the NW measured in (a), which defines regions, with the gradient SF density indicated by the red arrow. (c)–(e) HRTEM images at positions indicated by squares in (b). The nanowire is imaged along the $[2\bar{1}\bar{1}0]$ zone axis. Yellow arrows point to the ZB (111) microfacets. (f) Stacking fault density at the positions where spectra in (a) were measured. (g) Fitted LO mode integrated area, measured in (a), normalized to the total area as a function of the stacking fault density concluded from (f).

crystal structure, with the lower part having only a few SFs (1–20 SFs/250 nm) and the upper part exhibiting an increasing density of SFs (30–120 SFs/250 nm) towards the tip. Between the two segments all NWs have a pure ZB segment which we discuss later. Figures 1(d) and 1(e) show representative Raman spectra recorded at positions in the high- and low-SF-density regions, respectively. In both cases the expected WZ InAs peaks E_2, $A_1 + E_1$(TO), and $A_1 + E_1$(LO), at 211, 215, and 238 cm^{-1}, respectively, are clearly seen. Obviously, the spectrum measured from a high-SF-density area shows a significant LO peak compared with the spectrum from an area with a low SF density ($\sim$1/250 nm). The peak marked with an asterisk has an unknown origin but could be either a B_1 mode [29] or a splitting of the $A_1 + E_1$(TO) mode. To evaluate further the effect of the SF density on the LO mode intensity, Raman spectra were measured at positions along the axis of a different NW with a 100 nm step size. The TEM image is presented in Fig. 2(b), and the corresponding Raman map in the vicinity of the LO mode is presented in Fig. 2(a). The SF density found from HRTEM measurements as shown in Figs. 2(c)–2(e) is plotted in Fig. 2(f) as a function of the scan position. The integrated area of the LO mode normalized to the total integrated area is extracted from the Raman scan and presented in Fig. 2(g) as a function of the SF density taken from Fig. 2(f). The LO mode integrated intensity clearly increases with increasing SF density. This trend was confirmed on five InAs NWs from the same growth as shown in Fig. 3(b). For these NWs, Raman spectra were recorded at fewer points and the TEM images had a lower resolution compared to the images in Fig. 2, making it difficult to resolve all SFs in the high-density region. This accounts for the lower maximum value of the SF density scale in Fig. 3 compared to Fig. 2(g). The observed dependence of the LO mode intensity on the SF density is an indication that the forbidden LO mode in the Raman spectrum is indeed enhanced by stacking variation in the NW crystal structure.

It is well established that the forbidden LO mode can be induced by resonance when the photon energy is close to an electronic transition [35]. In the following we discuss the dependency of the LO mode intensity on the SF density for different laser photon energies to investigate the effect of resonance. In InAs, the relevant resonance is associated with the E_1 electronic band gap since its energy is in the optical range [36]. For InAs NWs, however, the situation is complicated by the fact that the band structure depends on the crystal structure, which can be either ZB, WZ, or a mixture. Resonant Raman spectroscopy of ZB InAs in bulk form was studied in Refs. [37] and [38], where the resonance of the LO mode was experimentally found at $\sim$2.65 eV ($\sim$467.8 nm). For InAs NWs, the calculated E_1 gap was found at $\sim$2.568 eV ($\sim$482.8 nm) and $\sim$2.432 eV ($\sim$509.8 nm) for the ZB and WZ structure, respectively [39]. However, different

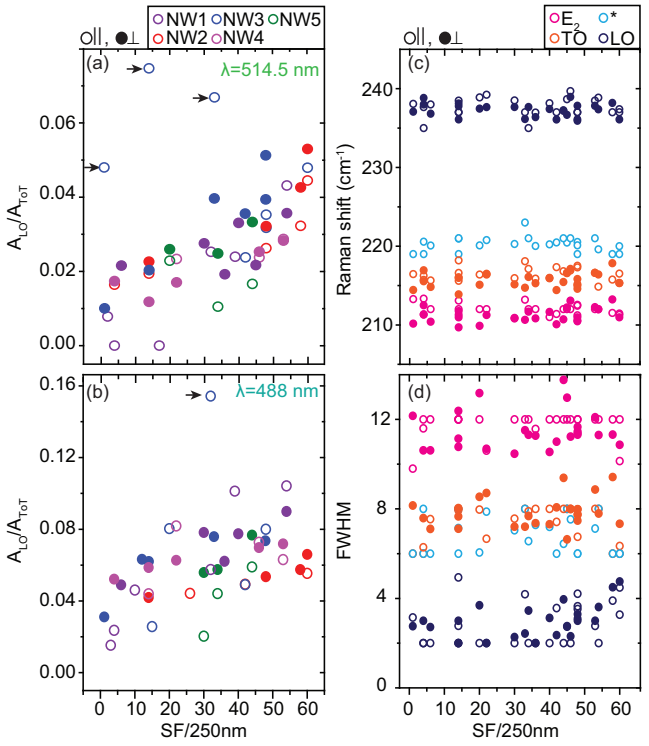

FIG. 3. (a) LO mode integrated area normalized to the total area for five individual InAs NWs as a function of the stacking fault density calculated using TEM images of the same NWs. Open and filled symbols indicate excitation polarization parallel and perpendicular to the NW axes, respectively, at a 514.5 nm excitation wavelength. (b) Same as (a) except the excitation wavelength is 488 nm. Arrows indicate data points from NW3, where an unusually high LO intensity was measured (see text). (c), (d) Raman shift and FWHM, respectively, for all NWs as a function of the stacking fault density at a 514.5 nm excitation wavelength.

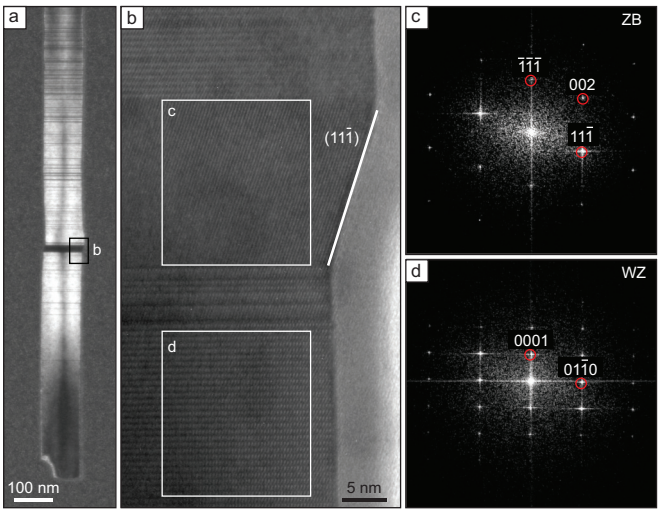

FIG. 4. (a) Dark-field TEM image, using the diffraction spot (01$\bar{1}$0), of NW 3. (b) HRTEM of the position marked in (a). (c), (d) FFTs of areas marked in (b). TEM images are acquired along the [2$\bar{1}\bar{1}$0]-zone axis.

experimental values have been reported [34,36,39]. In these studies NWs always contained a high SF density. To the best of our knowledge, no experimental report exists on pure NWs. We performed measurements at 514.5 and 488 nm excitation energies, which should be close to resonance for the WZ and ZB structures, respectively. We also measured one nanowire (NW1; Fig. 1) with a 632.8 nm (1.96 eV) excitation, significantly below the E_1 gap for both WZ and ZB. For 632.8 nm, no LO peak was detected at any point of the NW, consistent with previous measurements of high-SF-density WZ NWs at a similar excitation [34,36]. We attribute this observation to the asymmetric resonance profile of the allowed LO mode [37] where the Raman cross section drops considerably for energies below resonance. Figures 3(a) and 3(b) present the SF density dependency of the LO mode normalized integrated area for the 514.5 and the 488 nm excitation energies, respectively. As discussed below, a significant spread of intensities is observed, however, in both cases a clear positive trend is realized, and from a linear fit, comparable slopes of $5.1 \pm 0.6 \times 10^{-4}$ and $5.9 \pm 1.4 \times 10^{-4}$ $(\mathrm{SF}/250)^{-1}$ were found for the 514.5 and the 488 nm excitation energies, respectively. The spread of the data could be due to the SF counting method, which ignores the exact ratio of the ZB/WZ content by considering an SF as a change in growth sequence regardless of its actual size. Within this spread the resolution of the detected SFs could be estimated as ~30 SF/250.

The results in Figs. 1–3 establish a clear connection between the LO mode intensity and the SF density in the NW. In the following we discuss the possible mechanism causing this effect. One possible explanation is a crystal-defect-induced relaxation of the conventional limitation of only $q = 0$ phonons participating in Raman scattering [27,29,40]. In this case a downshift and broadening of the Raman line are expected for increasing SF density due to the phonon dispersion. These features were not observed in the peak positions and widths as shown in Figs. 3(c) and 3(d), respectively. Therefore, we believe that the effect of relaxation of the zone-center phonon condition has a minor effect on the observation of the LO mode. In Ref. [15] it was suggested that the crystal structure associated with the SF may also activate the LO mode in the Raman spectrum, as the most common SF type is a ZB inclusion, and according to the Raman selection rules the LO mode is allowed from the (111) planes. Thus, the measured LO signal could be a consequence of scattering from the (111) planes in the ZB segments. An observation consistent with such a mechanism comes from the investigation of the structure of the NW at the positions marked by arrows in Figs. 3(a) and 3(b), showing unusually high LO intensities. The corresponding HRTEM analysis is presented in Fig. 4. Two distinct regions are found: pure ZB and WZ labeled "c" and "d" and verified by the fast Fourier transform (FFT) of the HRTEM presented in Figs. 4(c) and 4(d), respectively. Here we have the biggest ZB inclusion in all measured NWs with a clear {111}-type facet. The TEM study of the measured NWs [e.g., Figs. 2(c) and 2(d)] confirmed the {111}-type microfacets associated with most of the investigated SFs. Since every single SF consists of a (111) plane at least three atomic bilayer rows thick, this explanation is valid also when a shorter SF exists in the NW. As a control experiment we performed Raman measurements on ZB InAs NWs with periodic twinning as

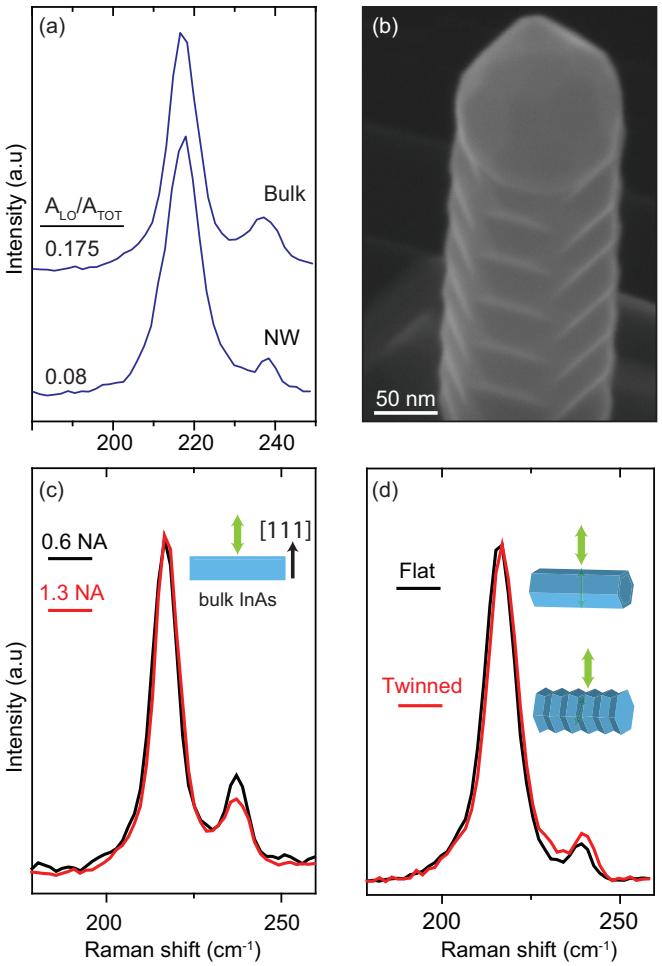

FIG. 5. (a) Perpendicularly polarized Raman spectra of a bulk ZB InAs sample with a [111] surface and InAs NWs with periodic twins forming a zigzag of {111} surface facets. (b) Scanning electron microscopic image of the InAs NW with periodic twinning. (c) Raman spectra of a bulk InAs sample as illustrated in the sketch recorded with two different NAs. (d) Raman spectra of ZB InAs NWs with and without periodic twinning as illustrated. Measurements were performed at 514.5 nm, and a linear baseline was subtracted from the data.

presented in the SEM image in Fig. 5(b). In these NWs, 15 nm segments with the {111}-type surface facet group are periodically stacked. Thus, these NWs correspond to the extreme limit of 100% stacking defect density. Figure 5(a) shows the Raman spectra of such a NW and a bulk sample with the same surface measured with the 514.5 nm excitation wavelength. The normalized integrated area of the LO mode averaged over four NWs was found to be around 0.08, and 0.175 for the bulk sample. Indeed, for the NWs this value is close to the maximum value measured in Fig. 3(a), which indicates that the observed LO mode is mainly induced by SFs due to their crystal structure. We believe that the detection from the (111) plane in the NW is enhanced by a combination of two mechanisms. First, the nonparallel part of the beam resulting from the focusing effect of the high NA objective [41] enhances scattering from the (111) planes. The contribution of this effect is verified by measuring from a (111) surface of a bulk InAs sample with two different NA objectives. As shown in Fig. 5(c) the LO mode is higher for the lower NA, where polarization distribution is more uniform and better aligned to the surface. Second, another mechanism is light refraction off the twinned surface, causing a deflection in the light path in the NW which enhances polarization alignment to the (111) planes in the NW. This is supported by comparing a Raman signal from a ZB NW with and without periodic microfacets as illustrated in Fig. 5(d) and a higher LO peak is observed from the NW with twins. In general, due to the imperfection of backscattering from a NW the LO mode could be activated from the (111) planes in the ZB inclusions in a WZ-dominant structure.

B. GaAs nanowires

To complete this study and complement the conclusions made for InAs, we present in the following a similar set of experiments for GaAs NWs which have the same crystal structure as InAs but a different electronic band structure and therefore different resonance conditions. Raman and TEM measurements were performed on four WZ GaAs NWs [42]. The NWs consist of two parts; one half is SF free and the other half exhibits an increasing SF density, with a maximum SF density of ∼25 SF/250 nm, lower than in the InAs case. A typical NW structure is shown in the TEM image in Fig. 6(a). Figure 6(b) shows that Raman spectra recorded in an SF-free and in high-SF-density areas again reveal a dependency of the LO peak (appearing at 286 cm^{-1}) intensity on the SF density in the NW. The figure also shows the Raman TO* peak at ∼264 cm^{-1}. Similarly to Figs. 3(a) and 3(b) the integrated area of the LO mode is normalized to the total integrated area and presented in Fig. 6(c) for three wavelengths: 632.8, 514.5, and 488 nm. For GaAs the 632.8 nm line is close to resonance with the fundamental band gap [43,44]. Again, the SF density affects the LO mode intensity, as the positive trend is clear for parallel excitation. Note that the maximum SF density is considerably lower than in the InAs case, making trends less obvious. For perpendicular polarization the LO integrated area is at its maximum all over the NW. We attribute this behavior to the polarization dependency of the dipole-allowed optical transitions, where for perpendicular polarization more transitions are allowed, which enhances the resonance effect [45]. In the case of GaAs, a positive trend was observed for both 514.5 and 488 nm excitations (away from resonance). Interestingly, at 488 nm we observe an almost-vanishing LO mode in the pure WZ part. This indicates that Raman spectroscopy is a promising optical technique to resolve even a few stacking faults under suitable measurement conditions. At 488 nm excitation only one NW was measured due to the extremely weak signal from the NWs.

Finally, we consider the Raman response of the pure ZB tip of the GaAs NW in Fig. 6(a). An HRTEM image is presented in Fig. 6(e), with the inset showing an FFT from the same area. The pyramid-shaped tip has {110}-type facets. The Raman spectrum of the tip is presented in Fig. 6(d), where the allowed E_2 and $E_1 + A_1$(TO) modes are observed at 257.5 and 266.4 cm^{-1}, and the forbidden $E_1 + A_1$(LO) mode at 290.6 cm^{-1}. Here, the E_2 mode may correspond to the WZ area below the tip. Two additional peaks clearly appear in the spectrum at

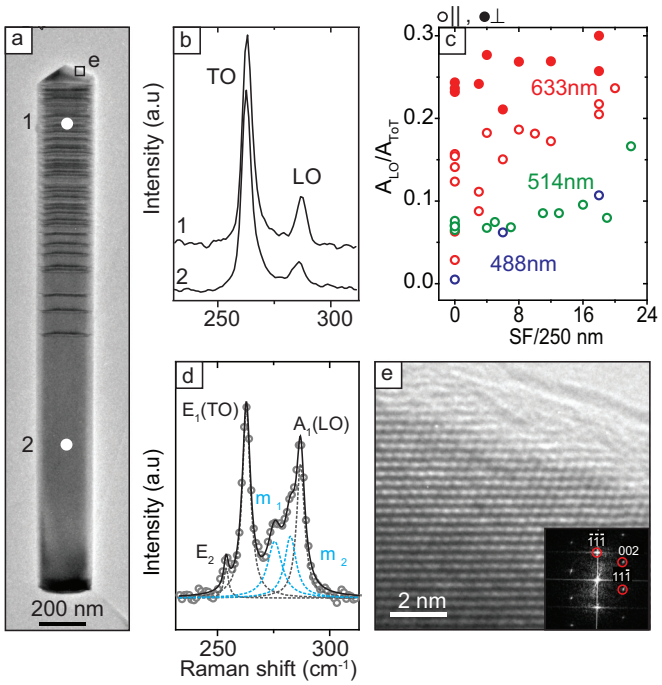

FIG. 6. (a) TEM image of a GaAs NW. The bottom part of the NW is SF-free, whereas the other half exhibits a gradient in SF density. (b) Raman spectra measured of areas marked in (a) at 632.8 nm and for parallel excitation polarization. (c) Integrated area of the LO mode normalized by the total area of five individual NWs measured at 632.8, 514.5, and 488 nm excitation wavelengths and for excitation polarization parallel (open circles) and perpendicular (filled circles) to the NW axes. (d) Raman spectrum of the tip of the NW shown in (a) measured at 632.8 nm for parallel excitation polarization. (e) HRTEM image from the NW tip marked in (a) showing a pure ZB crystal structure. Inset: An FFT from the same area.

279.1 and 286.1 cm^{-1}, denoted m_1 and m_2, respectively. These frequencies do not match the WZ or ZB GaAs phonons [15]; possibly, m_1 could be an enhanced surface mode and m_2 the $E_1 + A_1$(LO) mode splitting. Similar spectra were observed at the tip of all measured NWs. The Raman spectrum of the tip represents a good example of the imperfect scattering causing detection of phonon modes beyond the selection rules.

IV. CONCLUSION

In conclusion, we have investigated the relationship between the intensity of the forbidden LO phonon mode and the density of SFs in WZ InAs and GaAs NWs by combining TEM and micro-Raman mapping in individual NWs with graded SF densities. A clear dependency of the LO mode intensity on the SF density was observed in different resonance regimes. Accounting for the effects of the optical elements and the nanowire morphology, the results were found to be consistent with an LO mode induced by the (111) crystal plane of the ZB-type SFs. The study shows that the intensity of the forbidden LO in the Raman spectrum can be used for locally investigating the relative variation of stacking fault densities either along single nanowires or between nanowires. Such information may prove useful for rapid screening of nanowire samples and for selecting pure segments of nanowires suitable for electrical devices.

ACKNOWLEDGMENTS

We thank the Danish Agency for Science Technology and Innovation (The Danish Council for Strategic Research—ANaCell project), Center for Synthetic Biology, Copenhagen University, funded by the UNIK research initiative of the Danish Ministry of Science, Technology, and Innovation (Grant No. 09-065274), bioSYNergy, the University of Copenhagen's Excellence Programme for Interdisciplinary Research, the Lundbeck Foundation, the Villum Foundation, and the Carlsberg Foundation. The Center for Quantum Devices is supported by the Danish National Research Foundation.This work was also supported by the Swedish Research Council (V.R.) and the Knut and Alice Wallenberg Foundation (K.A.W.).

[1] M. Bjork, B. Ohlsson, T. Sass, A. Persson, C. Thelander, M. Magnusson, K. Deppert, L. Wallenberg, and L. Samuelson, Nano Lett. **2**, 87 (2002).
[2] C. Thelander, M. Bjork, M. Larsson, A. Hansen, L. Wallenberg, and L. Samuelson, Solid State Commun. **131**, 573 (2004).
[3] A. Das, Y. Ronen, Y. Most, Y. Oreg, M. Heiblum, and H. Shtrikman, Nat. Phys. **8**, 887 (2012).
[4] L. Hofstetter, S. Csonka, J. Nygard, and C. Schoenenberger, Nature **461**, 960 (2009).
[5] J. van Dam, Y. Nazarov, E. Bakkers, S. De Franceschi, and L. Kouwenhoven, Nature **442**, 667 (2006).
[6] S. Nadj-Perge, S. M. Frolov, E. P. A. M. Bakkers, and L. P. Kouwenhoven, Nature **468**, 1084 (2010).
[7] V. Mourik, K. Zuo, S. M. Frolov, S. R. Plissard, E. P. A. M. Bakkers, and L. P. Kouwenhoven, Science **336**, 1003 (2012).
[8] M. T. Deng, C. L. Yu, G. Y. Huang, M. Larsson, P. Caroff, and H. Q. Xu, Nano Lett. **12**, 6414 (2012).
[9] Y. Cui, Q. Wei, H. Park, and C. Lieber, Science **293**, 1289 (2001).
[10] P. Krogstrup, H. I. Jorgensen, M. Heiss, O. Demichel, J. V. Holm, M. Aagesen, J. Nygard, and A. Fontcuberta i Morral, Nat. Photon. **7**, 306 (2013).
[11] Y. Cui, Z. Zhong, D. Wang, W. Wang, and C. Lieber, Nano Lett. **3**, 149 (2003).
[12] H. Ng, J. Han, T. Yamada, P. Nguyen, Y. Chen, and M. Meyyappan, Nano Lett. **4**, 1247 (2004).
[13] C. Yeh, Z. Lu, S. Froyen, and A. Zunger, Phys. Rev. B **46**, 10086 (1992).
[14] D. Spirkoska, J. Arbiol, A. Gustafsson, S. Conesa-Boj, F. Glas, I. Zardo, M. Heigoldt, M. H. Gass, A. L. Bleloch, S. Estrade, M. Kaniber, J. Rossler, F. Peiro, J. R. Morante, G. Abstreiter, L. Samuelson, and A. Fontcuberta i Morral, Phys. Rev. B **80**, 245325 (2009).
[15] I. Zardo, S. Conesa-Boj, F. Peiro, J. R. Morante, J. Arbiol, E. Uccelli, G. Abstreiter, and A. Fontcuberta i Morral, Phys. Rev. B **80**, 245324 (2009).

[16] P.-A. Mante, S. Lehmann, N. Anttu, K. A. Dick, and A. Yartsev, Nano Lett. **16**, 4792 (2016).
[17] Z. Zanolli, F. Fuchs, J. Furthmüller, U. von Barth, and F. Bechstedt, Phys. Rev. B **75**, 245121 (2007).
[18] K. A. Dick, P. Caroff, J. Bolinsson, M. E. Messing, J. Johansson, K. Deppert, L. R. Wallenberg, and L. Samuelson, Semicond. Sci. Technol. **25**, 024009 (2010).
[19] J. Johansson, K. A. Dick, P. Caroff, M. E. Messing, J. Bolinsson, K. Deppert, and L. Samuelson, J. Phys. Chem. C **114**, 3837 (2010).
[20] S. Lehmann, J. Wallentin, D. Jacobsson, K. Deppert, and K. A. Dick, Nano Lett. **13**, 4099 (2013).
[21] H. J. Joyce, J. Wong-Leung, Q. Gao, H. H. Tan, and C. Jagadish, Nano Lett. **10**, 908 (2010).
[22] P. Caroff, K. A. Dick, J. Johansson, M. E. Messing, K. Deppert, and L. Samuelson, Nat. Nanotech. **4**, 50 (2009).
[23] M. Nilsson, L. Namazi, S. Lehmann, M. Leijnse, K. A. Dick, and C. Thelander, Phys. Rev. B **93**, 195422 (2016).
[24] M. D. Schroer and J. R. Petta, Nano Lett. **10**, 1618 (2010).
[25] C. Thelander, P. Caroff, S. Plissard, A. W. Dey, and K. A. Dick, Nano Lett. **11**, 2424 (2011).
[26] M. Timofeeva, A. Bouravleuv, G. Cirlin, I. Shtrom, I. Soshnikov, M. Reig Escalé, A. Sergeyev, and R. Grange, Nano Lett. **16**, 6290 (2016).
[27] F. J. Lopez, E. R. Hemesath, and L. J. Lauhon, Nano Lett. **9**, 2774 (2009).
[28] J. K. Panda, A. Roy, A. Singha, M. Gemmi, D. Ercolani, V. Pellegrini, and L. Sorba, Appl. Phys. Lett. **100**, 143101 (2012).
[29] N. G. Hörmann, I. Zardo, S. Hertenberger, S. Funk, S. Bolte, M. Döblinger, G. Koblmüller, and G. Abstreiter, Phys. Rev. B **84**, 155301 (2011).
[30] M. H. Magnusson, K. Deppert, J.-O. Malm, and L. Samuelson, Nanostruct. Mater. SI **12**, 45 (1999).
[31] C. Lindberg, A. Whiticar, K. A. Dick, N. Sköld, J. Nygård, and J. Bolinsson, Nano Lett. **16**, 506 (2016).
[32] R. Tanta, T. Kanne, F. Amaduzzi, Z. Liao, M. H. Madsen, E. Alarcón-Lladó, P. Krogstrup, E. Johnson, A. Fontcuberta i Morral, T. Vosch, J. Nygård, and T. S. Jespersen, Nanotechnology **27**, 305704 (2016).
[33] PELCO 21509-10, silicon nitride support film, 50 nm with nine each 0.1 × 0.1 mm windows.
[34] M. Möller, M. M. De Lima, A. Cantarero, L. C. O. Dacal, J. R. Madureira, F. Iikawa, T. Chiaramonte, and M. A. Cotta, Phys. Rev. B **84**, 085318 (2011).
[35] M. Cardona, *Light Scattering in Solids I. Topics in Applied Physics*, Vol. 8 (Springer, Berlin, 1983).
[36] I. Zardo, S. Yazji, N. Hörmann, S. Hertenberger, S. Funk, S. Mangialardo, S. Morkötter, G. Koblmüller, P. Postorino, and G. Abstreiter, Nano Lett. **13**, 3011 (2013).
[37] G. Rubloff, E. Anastassakis, and F. Pollak, Solid State Commun. **13**, 1755 (1973).
[38] R. Carles, N. Saint-Cricq, J. B. Renucci, A. Zwick, and M. A. Renucci, Phys. Rev. B **22**, 6120 (1980).
[39] J. K. Panda, A. Chakraborty, D. Ercolani, M. Gemmi, L. Sorba, and A. Roy, Nanotechnology **27**, 415201 (2016).
[40] I. Campbell and P. Fauchet, Solid State Commun. **58**, 739 (1986).
[41] Q. Li, I. Ledoux-Rak, and N. D. Lai, Adv. Device Mater. **1**, 4 (2015).
[42] The WZ structure is confirmed by diffraction patterns which are not shown in the paper.
[43] B. Ketterer, M. Heiss, M. J. Livrozet, A. Rudolph, E. Reiger, and A. Fontcuberta i Morral, Phys. Rev. B **83**, 125307 (2011).
[44] R. Trommer and M. Cardona, Phys. Rev. B **17**, 1865 (1978).
[45] B. Ketterer, M. Heiss, E. Uccelli, J. Arbiol, and A. Fontcuberta i Morral, ACS Nano **5**, 7585 (2011).